PAPER • **OPEN ACCESS**

The influence of annealing atmosphere on sputtered indium oxide thin-film transistors

To cite this article: Na Xiao *et al* 2023 *J. Phys. D: Appl. Phys.* **56** 425102

OPEN ACCESS
IOP Publishing
Journal of Physics D: Applied Physics
J. Phys. D: Appl. Phys. **56** (2023) 425102 (10pp)
https://doi.org/10.1088/1361-6463/ace6b8

The influence of annealing atmosphere on sputtered indium oxide thin-film transistors

Na Xiao[1,*], Saravanan Yuvaraja[1], Dhanu Chettri[1], Zhiyuan Liu[1], Yi Lu[1], Chehao Liao[2], Xiao Tang[1] and Xiaohang Li[1,*]

[1] Advanced Semiconductor Laboratory, Electrical and Computer Engineering Program, CEMSE Division, King Abdullah University of Science and Technology (KAUST), Thuwal 23955-6900, Saudi Arabia
[2] Department of Electronic Engineering, National Yunlin University of Science and Technology, Yunlin, Taiwan

E-mail: na.xiao@kaust.edu.sa and xiaohang.li@kaust.edu.sa

Received 1 March 2023, revised 30 June 2023
Accepted for publication 12 July 2023
Published 24 July 2023

Abstract

Indium oxide (In_2O_3) thin films sputtered at room temperature were annealed under different atmospheres and examined for thin-film transistor (TFT) active channel applications. The annealing process was performed in a rapid thermal annealing system at 350 °C under O_2, Ar, forming gas (FG, 96% N_2/4% H_2), and N_2. It was found that the annealed In_2O_3 TFTs exhibited high field-effect mobility ($\mu_{FE} > 40$ cm^2 V^{-1}s^{-1}), high on/off current ratio ($I_{on/off} \sim 10^8$), and controlled threshold voltage (V_{TH}) for the enhancement- and depletion-mode operations. Note that the annealing atmosphere has a significant effect on the electrical performance of the In_2O_3 TFTs by inducing changes in oxygen-related species, particularly oxygen vacancies (V_O) and hydroxyl/carbonate species (O–H/C–O). For the O_2-, Ar-, FG-, and N_2-annealed TFTs, μ_{FE} was in increasing order accompanied by a negative shift in V_{TH}, which is a result attributed to the larger V_O in the In_2O_3 thin films. Furthermore, the ΔV_{TH} of the FG-, and N_2-annealed TFTs in a positive bias stress test was greater than that of the O_2-, Ar-annealed devices, attributing to their lower density of O–H/C–O groups in the In_2O_3 thin films. Our results suggest that the annealing atmosphere contributes to the internal modifications of the In_2O_3 structure and in turn altered the electrical characteristics of TFTs. These annealed In_2O_3 TFTs with high performance are promising candidates for realizing large-area, transparent, and high-resolution displays.

Supplementary material for this article is available online

Keywords: In_2O_3, thin-film transistor, oxide semiconductor, annealing atmosphere, bias stability

(Some figures may appear in colour only in the online journal)

* Authors to whom any correspondence should be addressed.

1. Introduction

Wide-bandgap oxide semiconductors (OSs) are widely investigated as promising channel layers of thin-film transistors (TFTs) in display technology [1, 2], artificial synapses [3], sensors [4], Schottky devices [5] and other applications [6–8]. Among them, indium–gallium–zinc oxide (IGZO) TFTs have become the backplane standard for active-matrix liquid-crystal displays and active-matrix organic light-emitting diode displays because of their reasonable mobility ($\mu_{FE} > 10$ cm^2 V^{-1}s^{-1}), high $I_{on/off}$ ratio ($>10^8$), extremely low leakage current ($<10^{-15}$ A), low process temperature (<350 °C), high uniformity, and large-area scalability [9–11]. To meet the requirements of ultra-high-resolution and high frame rate next-generation displays, various OS TFTs with higher mobility than IGZO TFTs have been extensively studied for next-generation display applications [12–14]. Among these transistors, In-rich OS TFTs are the most promising candidates because of their excellent high-mobility performance. The In 5s orbital having a large spatial spread and a large overlap provides a facile electron transport path, which, in addition to their low electron effective mass, endows In-rich OS TFTs with high electron mobility [14].

For most OS TFTs, the presence of oxygen-related species, such as oxygen vacancies (V_O) or hydroxyl/carbonate species (O–H/C–O), has a considerable impact on their electrical performance [15, 16]. Generally, V_O readily creates shallow or deep donor states in the oxide channel layer. These shallow donor states supply electrons to the conduction band (CB), leading to an increase in electron concentration. In contrast, the deep donor states in the subgap region act as trap states, degrading device performance [17–19]. In addition, oxygen bonds in O–H/C–O groups are considered to generate acceptor-like states near the CB edge and enhance electron trapping during positive bias stress (PBS) applications [20]. Therefore, multiple attempts have been made to modulate oxygen-related species in the active channel layer such as multi-cation doping [21, 22], changing the sputtering gas flow [23], annealing treatment [24], plasma treatment [25], or their combination [26, 27]. One of the effective routines for realizing TFTs with good performance is the deposition of OS channel layers with high resistivity, followed by a post-deposition annealing treatment. Annealing is one of the most commonly used methods for optimizing active channel layers because of its effectiveness in alleviating deep traps formed by ion bombardment or unintended defects during film deposition or the synthesis process [28]. Most previous studies demonstrated that the performance of TFTs under multiple annealing conditions varies depending on the channel material and process conditions chosen [29, 30]. Different annealing conditions, especially the annealing atmosphere, have a significant effect on the performance of OS TFTs. However, most studies on the effects of annealing conditions have focused on IGZO [31], indium–gallium–tin oxide (IGTO) [29], indium–zinc–tin oxide (IZTO) [32], indium-gallium oxide [33], and other In-based multi-cation composition OSs [34, 35]. Few studies have been conducted on the effect of the annealing atmosphere on the performance of In_2O_3 TFTs. Yuan *et al* reported that the sputtered In_2O_3 TFTs followed by a post-deposition annealing in vacuum or air showed significantly different mobilities; however, the fundamental mechanism behind the carrier mobility enhancement is unclear [36]. Si *et al* reported that In_2O_3 TFTs deposited by atomic layer deposition (ALD) and annealed in O_2, H_2, or N_2 respectively, produced similar results indicating that the annealing atmosphere had no effect on the performance of In_2O_3 TFTs [37]. However, ALD-processed and sputtered In_2O_3 thin films significantly differ in terms of aspects such as chemical composition and bonding state [38, 39]. Therefore, this conclusion cannot be inferred to be applicable to sputtered In_2O_3 TFTs. For OS TFTs, a complete understanding of the effects of the annealing atmospheres on their electrical properties and stability is required. In particular, stability under gate bias stress is important for OS TFT applications. This suggests the need to determine the most suitable annealing atmosphere for In_2O_3 thin films to improve the electrical properties of In_2O_3 TFTs. In this study, we deposited In_2O_3 thin films by sputtering at room temperature and investigated the effect of the annealing atmosphere on the electrical characteristics and bias stability of In_2O_3 TFTs.

2. Experimental details

The fabrication process of the devices is as follows. First, heavily doped p-type silicon (p^{++}-Si) substrates with 2 μm thermally grown SiO_2 were cleaned with acetone, isopropyl alcohol, and deionized water for 10 min each. Next, 30 nm Al was deposited using radio frequency (RF) magnetron sputtering as the gate metal. Then, 30 nm Al_2O_3 was grown as the gate dielectric at 250 °C using $(CH_3)_3Al$ (TMA) and O_2 plasma as Al and O precursors. Next, ∼10 nm In_2O_3 films were deposited by RF magnetron sputtering at room temperature as the active channel layer. In_2O_3 films with a thickness of ∼40 nm were then deposited on the SiO_2/Si substrates and sapphire substrates to examine their structural and optical properties. The sputtering power was 100 W, the O_2 and Ar gas flow ratios were set to 50%, and the working pressure was 10 mTorr. About 5 min pre-sputtering was performed to eliminate the contamination of the In_2O_3 target. Subsequently, 20 nm Ti and 100 nm Au were deposited by RF magnetron sputtering as the source and drain metal contacts, respectively. Finally, the Al_2O_3 was dry-etched using BCl_3 as the reactive gas to expose the underlying gate. The bottom gate, channel, and source/drain metals were fabricated by lithography, sputtering and lift-off processes. The channel length and width were 40 and 240 μm, respectively. The annealing process was performed in a rapid thermal annealing system under four different annealing atmospheres of O_2, Ar, forming gas (FG) and N_2. The annealing temperature and time were fixed at 350 °C and 1 min, respectively.

The surface morphology was characterized using an atomic force microscopy (AFM, Bruker Dimension Icon scanning probe microscope) in tapping mode. Film thickness was jointly determined by transmission electron microscope (TEM), AFM

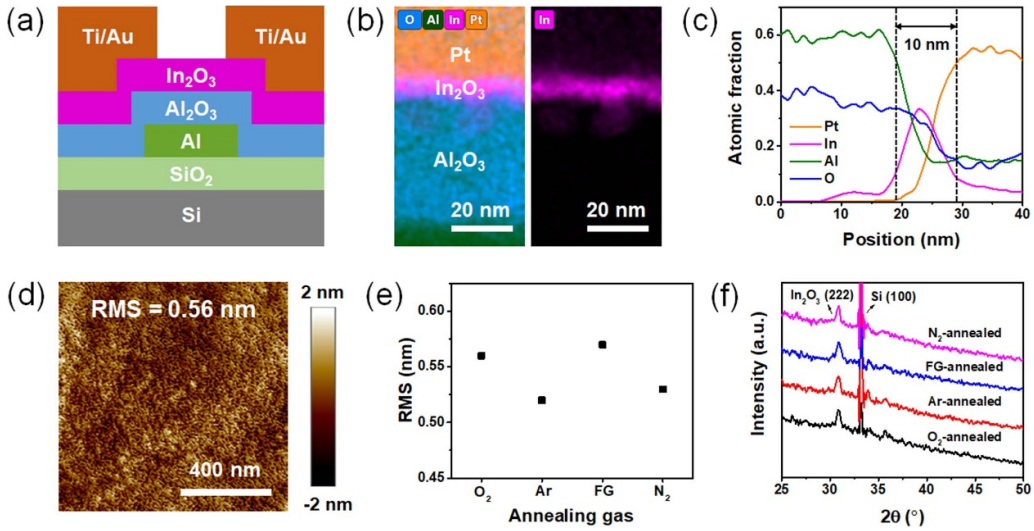

Figure 1. (a) Schematic of an In_2O_3 transistor. (b) HAADF-STEM cross-sectional image with EDX elemental mapping of an O_2-annealed In_2O_3 transistor, and (c) the corresponding cross-sectional profiles of the elements, confirming that the thickness of In_2O_3 film is ∼10 nm. (d) AFM image of the O_2-annealed In_2O_3 thin film. (e) Distribution of surface roughness RMS values extracted from AFM images under different annealing atmospheres. (f) XRD diffraction patterns of all annealed In_2O_3 thin films.

and ellipsometry. TEM lamella samples were prepared by focused ion beam (FIB) using a FEI Helios G4 scanning electron microscope. Before FIB milling, a platinum (Pt) layer was deposited to protect the sample surface from ion damage. The FEI Titan ST microscope system with an acceleration voltage of 300 kV was equipped with a Super-X energy-dispersive x-ray spectroscopy (EDX) for high-angle annular dark-field scanning transmission electron microscopy (HAADF-STEM) imaging. Crystal structures were studied using a Bruker D2 PHASER x-ray diffraction (XRD) system with a Cu tube source ($\lambda = 1.541\,84$ Å) at 30 kV. O 1s spectra were examined by x-ray photoelectron spectroscopy (XPS) was performed in a high vacuum using a Kratos Amicus XPS system equipped with a monochromatic Al Kα x-ray source operating at 10 kV. The electrical properties and gate bias stability of the fabricated TFTs were measured using a Keithley 4200 system and a Cascade Summit probe station at room temperature and ambient atmosphere.

3. Results and discussion

Figure 1(a) shows a schematic of an In_2O_3 TFT with a bottom-gate-top-contact structure fabricated on a Si substrate. The gate stack is structured with 30 nm Al as the bottom gate, 30 nm Al_2O_3 as the gate dielectric, ∼10 nm In_2O_3 as the channel layer, and 20/100 nm Ti/Au as the top source/drain contact. Figure 1(b) shows the HAADF-STEM with EDX mapping of the O_2-annealed In_2O_3 TFT, highlighting the Al/In/O elements. The top Pt layer was deposited to protect the top portion of the specimen from ion damage during sample preparation. The corresponding elemental profiles shown in figure 1(c) confirm that the thickness of the In_2O_3 thin film is ∼10 nm. The thickness of the In_2O_3 thin film was also jointly determined by ellipsometer and AFM measurements. Figure 1(d) shows the surface morphology image of the O_2-annealed In_2O_3 thin film, indicating a smooth surface. As shown in figure 1(e), the surface roughness root mean square (RMS) values of the O_2-, Ar-, FG-, and N_2-annealed In_2O_3 films extracted from the corresponding AFM images are 0.56, 0.52, 0.58, and 0.53 nm, respectively, indicating that the surface roughness of the annealed films does not depend on the different annealing atmospheres. Figure 1(F) shows the XRD diffraction pattern of the annealed In_2O_3 thin films on the SiO_2/Si substrate. A weak diffraction peak at ∼31.8° corresponding to the (222) diffraction pattern was observed for all annealed In_2O_3 thin films, indicating their crystallinity nature. The presence of a strong diffraction peak at ∼33.2° originates from the Si (100) substrate. The crystallinity of the In_2O_3 thin films was further confirmed by TEM analysis.

Figure 2(a) shows the UV–Vis transmission spectra of all annealed In_2O_3 thin films. These films were deposited on a sapphire substrate with a thickness of ∼40 nm. The result indicates that the transmittance of the films does not depend on the annealing atmosphere, and all films demonstrate almost full transmittance in the visible region. Figure 2(b) shows the corresponding Tauc plots extracted from the transmission spectra. The optical bandgap (Eg) is determined using the Tauc's relation [40, 41]: $(ahv)^2 = A(hv - \mathrm{Eg})$, where a is the absorption coefficient, A is a constant, h is the Planck constant, and v is the frequency. Eg is extracted by extrapolating the linear part to the energy at $(ahv)^2 = 0$. Results indicate that the annealing atmosphere has no effect on the bandgap of the films because all annealed films exhibit the same Eg value of 3.71 eV.

To investigate the oxygen-related species in the In_2O_3 thin films annealed under different annealing atmosphere, XPS measurements were performed. As shown in figure 3, the O 1s

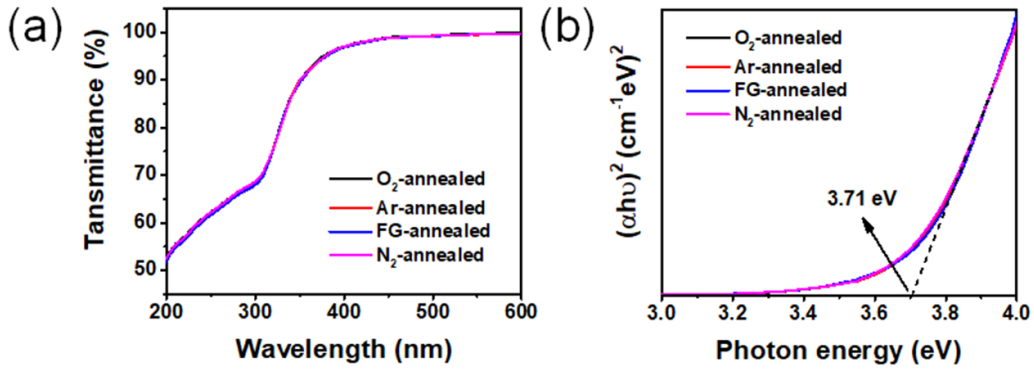

Figure 2. (a) UV–Vis transmittance spectra, and (b) corresponding extracted Tauc plots of In_2O_3 thin films.

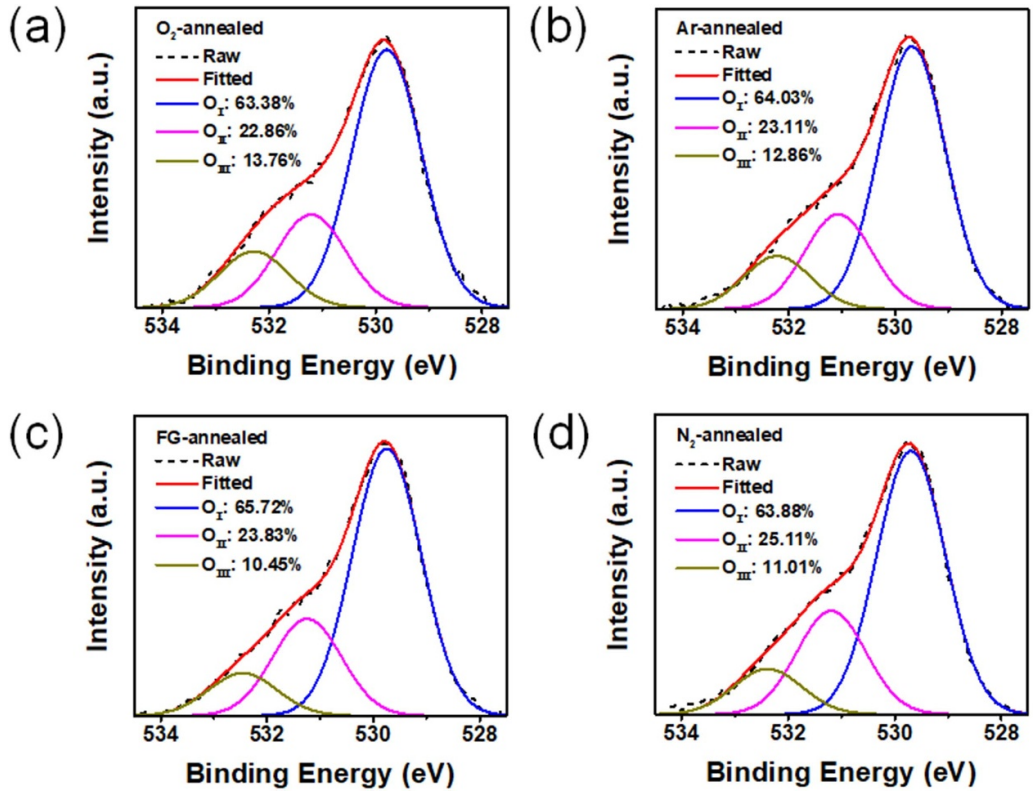

Figure 3. O 1s spectra of In_2O_3 thin films annealed under (a) O_2, (b) Ar, (c) FG, and (d) N_2 atmospheres, respectively.

peak was deconvoluted into three peaks centered at 529.7 eV (O_I), 531.3 eV (O_{II}), and 532.4 eV (O_{III}), corresponding to the oxygen in the In–O, V_O, and O–H/C–O [42, 43], respectively. The peak area ratios of $O_{II}/(O_I + O_{II} + O_{III})$ were 22.86%, 23.11%, 23.83%, and 25.11% for the In_2O_3 thin films annealed under O_2, Ar, FG, and N_2 respectively. These results indicate the presence of a large number of V_O in the In_2O_3 thin films. The N_2- and O_2-annealed films have the largest and smallest number of Vo, respectively. Similar results have been reported regarding IGZO TFTs [44, 45]. In addition to V_O, the O–H/C–O component is an important criterion to determine the quality of the In_2O_3 thin films, as less O–H/C–O leads to reduced surface scattering and electron charge trapping [29, 46]. The peak area ratios of $O_{III}/(O_I + O_{II} + O_{III})$ of the In_2O_3 thin films annealed under O_2, Ar, FG, and N_2 were 13.76%, 12.86%, 10.45%, and 11.01%, respectively. To summarize, the O_2-annealed In_2O_3 thin film has the smallest Vo and the largest O–H/C–O component, whereas the Ar-annealed In_2O_3 thin film exhibits moderate V_O and O–H/C–O component. Both N_2- and FG-annealed films exhibit smaller O–H/C–O components, whereas the V_O component of the N_2-annealed In_2O_3 thin film is larger than that of the FG-annealed In_2O_3 thin film.

Table 1 lists the elemental concentrations of the In_2O_3 thin films annealed under different atmospheres. The In/O atomic ratios of the annealed In_2O_3 thin films are in increasing order of the annealing atmosphere of O_2, Ar, FG, and N_2, respectively. Moreover, even for the smallest atomic ratio (1:1.39) of the In_2O_3 thin film annealed in O_2, it is still larger than that (1:1.5) of stoichiometric In_2O_3. This reveals that sputtered In_2O_3 thin films are typically rich in V_O.

Table 1. Elemental concentrations of In_2O_3 thin films annealed under different atmospheres.

Annealing atmosphere	In	O	Atomic ratio of In:O
O_2	41.92%	58.08%	1:1.39
Ar	43.61%	56.39%	1:1.29
FG	43.80%	56.20%	1:1.28
N_2	44.07%	55.93%	1:1.27

Figures 4(a) and (b) shows the representative I_D–V_{GS} characteristics of In_2O_3 TFTs annealed under different atmosphere on linear (V_{DS} = 0.1 V) and logarithmic (V_{DS} = 10 V) scales, respectively. Here, the enhancement mode is defined as V_{TH} >0 V, whereas the depletion mode is the opposite. Using linear extrapolation, the V_{TH} of the O_2-, Ar-, FG-, and N_2-annealed In_2O_3 TFTs are 1.7, 0.7, −1.1 and −2.8 V, respectively. This result indicates that enhancement- and depletion-mode operation of In_2O_3 TFTs can be selectively achieved under different post-deposition annealing atmospheres. The $I_{on/off}$ ratio of the O_2-, Ar-, and FG-annealed TFT is $\sim 10^8$, with the FG-annealed TFT exhibiting a slightly higher I_{off}. In contrast, the N_2-annealed In_2O_3 TFT exhibited undesired switching characteristics that are not completely depleted at a reasonable gate bias. Note that the gate leakage current (I_G) for all annealed samples exhibits low values of $\sim 10^{-11}$ A, which is the minimum current detection limit of our Keithley 4200 system. Figures 4(c)–(f) shows the representative I_D–V_{DS} characteristics of In_2O_3 TFTs annealed under different atmosphere. All annealed TFTs exhibit good operation in the n-channel mode with clear pinch-off voltages and saturation drain currents. The linear increase in I_D in the low drain voltage region shows a good ohmic contact between the channel layer and the source/drain contact. I_D obtained at V_{GS} of 10 V is 2.2, 2.7, 3.9, and 5.6 mA in increasing order for the O_2-, Ar-, FG-, and N_2-annealed In_2O_3 TFTs, respectively. The reference as-deposited In_2O_3 TFT was also measured, and the corresponding I_D–V_{GS} and I_D–V_{DS} curves are shown in figure S1. Compared to the annealed samples, the as-deposited In_2O_3 TFT shows undesirable electrical performance with a larger V_{TH} (6.8 V) and lower I_D (0.011 mA) at V_{GS} of 10 V under the same V_{DS} sweeping condition. Similar results have been reported for IGZO [47], IZTO [32], and InSnO [48] TFTs. It is known that the OS thin films deposited at room temperature typically have a loose structure that exhibits carrier scattering caused by poor film quality, resulting in few free carriers in the films and low conductivity and mobility. The electrical performance of the films can be greatly improved by promoting oxygen diffusion from the OS channel layer and rearrangement of molecular bonds through post-deposition annealing [32, 47, 48].

Figures 5(a)–(d) summarizes the dependence of V_{TH}, μ_{FE}, I_D, and SS on the annealing atmosphere evaluated from over 20 devices on the same substrate. μ_{FE} was determined from the linear transfer characteristics from equation (1), $\mu_{FE} = Lg_m/(WC_{OX}V_{DS})$, where g_m is the transconductance, C_{OX} is the oxide capacitance of the gate dielectric, and W and L are the channel width and channel length, respectively. SS was determined from equation (2): $SS = (dV_{GS}/d\log I_{DS})_{MAX}$. I_D was defined as the I_D at a fixed V_{OV} ($V_{OV} = V_{GS} - V_{TH}$) of 8 V for V_{DS} = 0.1 V in the transfer characteristics. All annealed TFTs show narrow parameter distributions in a single batch of devices, which confirms their high uniformity. For TFTs annealed under O_2, Ar, FG, and N_2, μ_{FE}, I_D, and SS are in increasing order, accompanied by a negative shift in V_{TH}. The observed electrical results are consistent with XPS results shown in figure 3 as we assume that the condition of the In_2O_3 thin films is correlates with that of oxygen-related species, particularly V_O. The conducting electrons in the In_2O_3 thin films are mainly derived from V_O that act as shallow donor states. Thus, a high number of V_O indicates high carrier concentration, resulting in low V_{TH}, a high conductivity and mobility [49, 50]. However, a higher electron concentration promotes the formation of percolation conduction paths in OSs, making it a problem for TFTs to reach complete depletion. The O_2-annealed In_2O_3 TFT exhibits lower conductivity and mobility because O_2 fills certain V_O, resulting in a lower carrier concentration than those of the other films. The N_2-annealed In_2O_3 TFT only reached partial depletion because of an excessive carrier concentration, which is mainly attributed to the desorption of oxygen atoms during the N_2 annealing process resulting in a large amount of V_O in the In_2O_3 thin film [51]. These results are consistent with previous reports on IGZO and IGTO TFTs [29, 45]. The SS of the N_2-annealed In_2O_3 TFT is not provided because V_{TH} is so negative that SS cannot be meaningfully measured. The higher SS of N_2- and FG-annealed TFTs than that of the O_2- and Ar-annealed TFTs indicates their poorer gate control, which is mainly attributed to their higher carrier concentrations.

The dependence of gate bias stability on the annealing atmosphere was investigated with a positive bias value of 10 V and a stress time of 3000 s. During bias stress, the gate was biased at a fixed voltage value of 10 V, while the source and drain were grounded. Bias stability is evaluated by the variation of V_{TH}, which is determined using the linear extrapolation of the transfer curve at the maximum g_m point. Figures 6(a)–(d) show the evolution of the transfer characteristics of the In_2O_3 TFTs annealed under O_2, Ar, FG, and N_2, respectively. From these figures, the transfer curves shift almost parallel toward the positive direction as the stress time increases. The long-term rate of V_{TH} shift is significantly reduced with a clear directional difference, thus suggesting the rebalance of the rates of different degradation mechanisms [52]. From the V_{TH}–stress time curves in figure 6(e), the corresponding ΔV_{TH} of the O_2-, Ar-, FG-, and N_2-annealed TFTs are 4.8 V, 3.9 V, 3.3 V and 3.4 V, respectively, at a stress time of 3000 s. This ΔV_{TH} difference showed the same trend as the difference of relative area of the O_{III} component observed in the XPS analysis. Previous studies on OS thin films and TFTs have demonstrated that that O_{III} mainly originates from the oxygen in absorbed hydroxyl and carbonate species (O–H/C–O), which typically generate acceptor-like states near the CB edge and enhance electron trapping during PBS application because of their polar nature in OSs [29]. Therefore, the larger

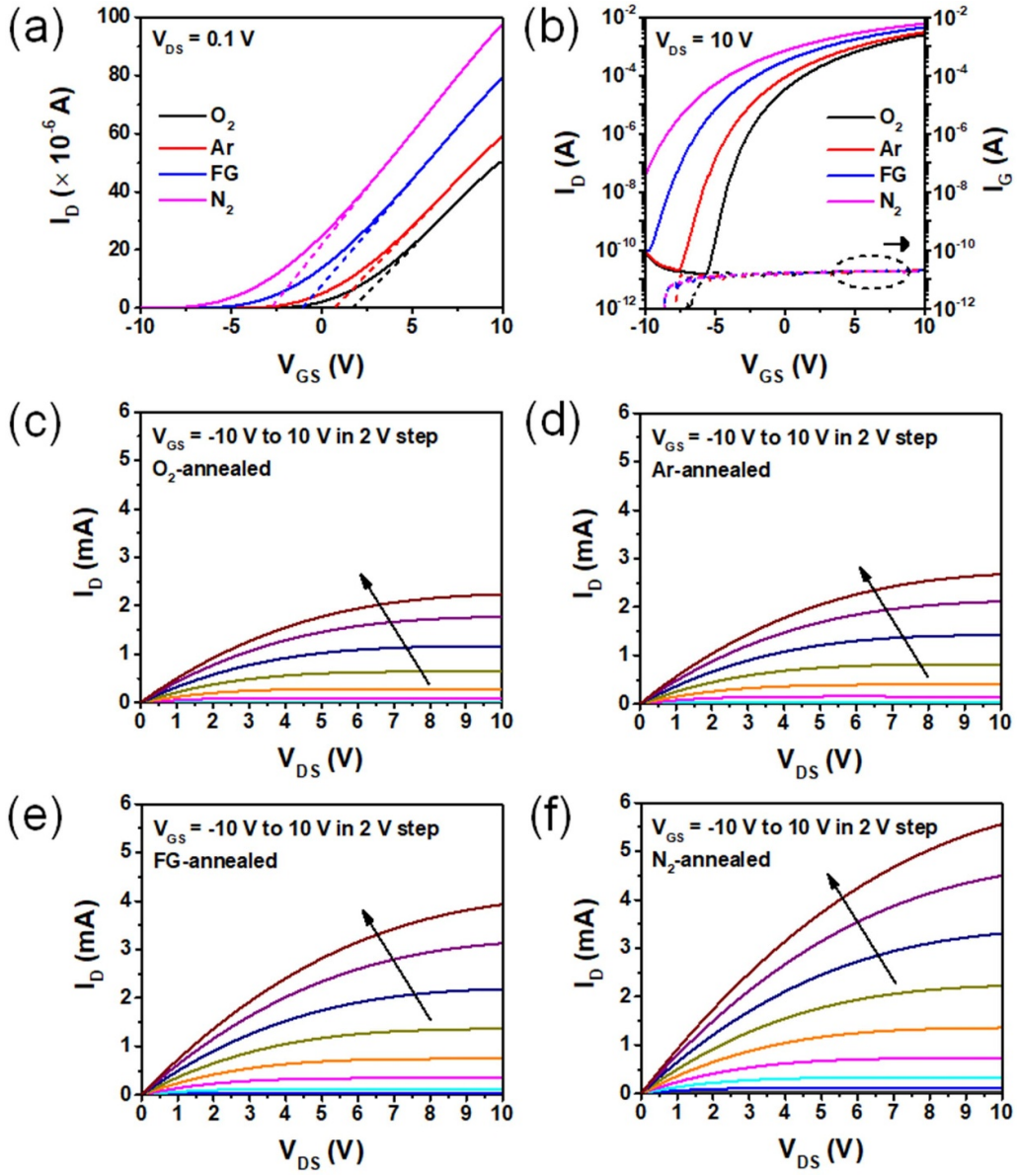

Figure 4. Representative (a) linear-scale and (b) log-scale I_D–V_{GS} characteristics of In_2O_3 TFTs prepared under different annealing atmospheres. Representative I_D–V_{DS} characteristics of (c) O_2-, (d) Ar-, (e) FG, and (f) N_2-annealed In_2O_3 TFTs.

ΔV_{TH} observed in the PBS tests of the O_2- and Ar-annealed In_2O_3 TFTs can be attributed to the higher density of O–H/C–O groups within the channel layer.

It is known that there are two factors that contribute to V_{TH} instability: (1) defect creation in the channel and (2) charge trapping in the dielectric and/or at the channel/insulator interface [53]. Defect creation typically results in the persistent degradation of sub-threshold slope and device mobility, whereas charge trapping does not [54]. The main difference between charge trapping at the interface and the injection into the dielectric is the amount of energy needed to remove the injected charge. Releasing the charge injected into a dielectric requires high energy and typically requires thermal annealing or the application of bias [55]. We observed that our devices can automatically relax to the original states within 4 h at room temperature after bias testing. The spontaneous recovery of V_{TH} after relaxation without any high energy and the negligible changes in SS shown in figure 6(f) suggest that charge trapping at the channel/insulator interface is the main reason for the instability of the In_2O_3 TFT PBS condition. The SS of the N_2-annealed In_2O_3 TFT is not provided in figure 6(f) because its large negative V_{TH} so that SS cannot be meaningfully measured.

The time-dependent V_{TH} observed during the PBS tests for the TFTs annealed under different atmospheres can be fitted using the stretched exponential equation:

$$\Delta V_{TH}(t) = \Delta V_{TH0}[1 - \exp[-(t/\tau)^{\beta}]]$$

where ΔV_{TH0} is ΔV_{TH} at infinite time, t is the stress time, β is the stretched-exponential exponent, and τ is the characteristic trapping time of the carriers, which correlates

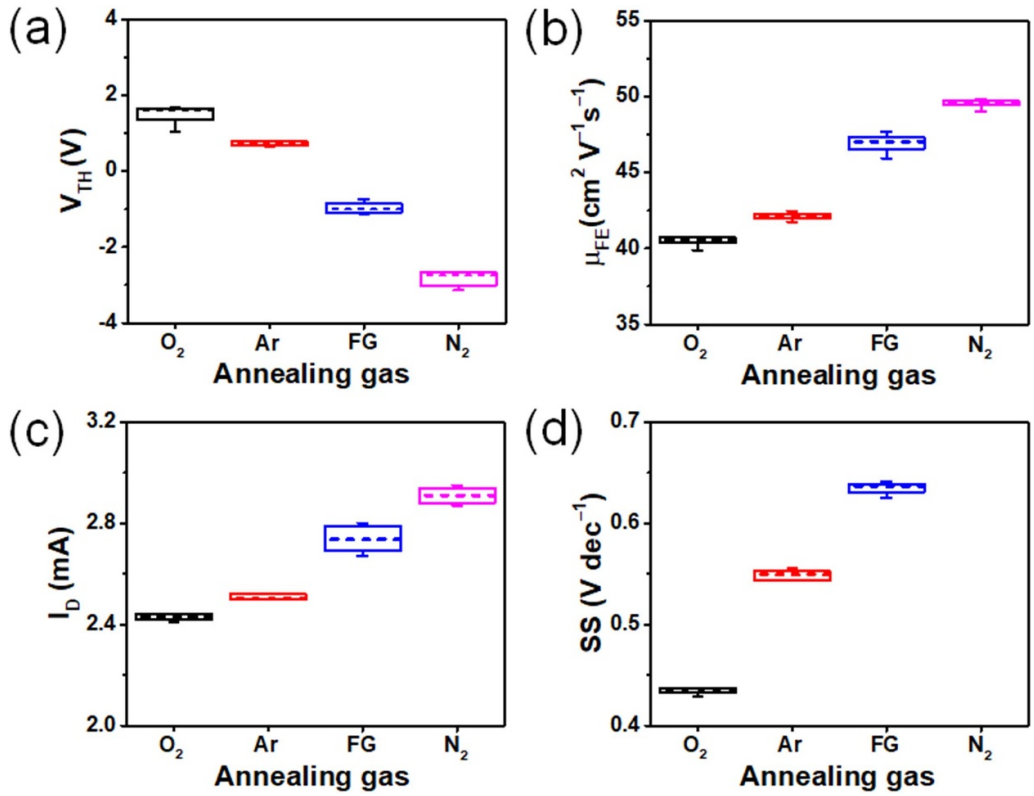

Figure 5. Dependence of the (a) V_{TH}, (b) μ_{FE}, (c) $I_{D,}$ and (d) SS of annealed In_2O_3 TFTs under different annealing atmospheres, respectively. The boxes are drawn with 25% of the data as the minimum and 75% as the maximum. The short horizontal lines correspond to the median line of the data.

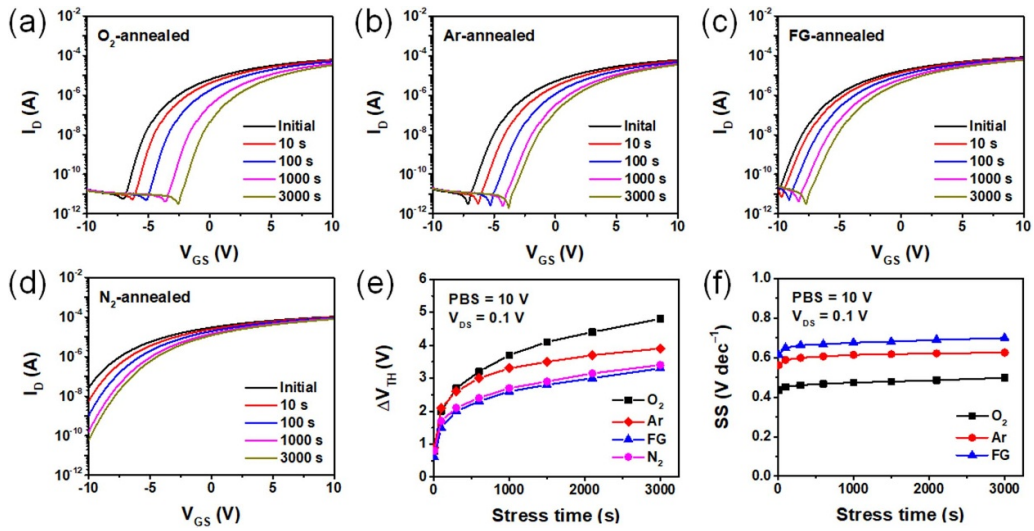

Figure 6. Evolution of transfer characteristics of In_2O_3 TFTs annealed in (a) O_2, (b) Ar, (c) FG, and (d) N_2 under PBS conditions. Variation in (e) ΔV_{TH} and (f) SS as a function of stress time.

with the average effective energy barrier [56, 57]. Table 2 lists the exacted fitting parameters from curve fitting for all TFTs. The In_2O_3 TFTs annealed under different atmospheres have different ΔV_{TH0}, τ and β, indicating different device degradation mechanisms, attributed to the generation of undesirable trap centers [52]. Furthermore, certain studies confirmed that the dynamic interaction between the exposed backchannel and the ambient atmosphere affects the V_{TH} stability of TFTs in PBS tests. The adsorbed oxygen can capture electrons from the CB, thus resulting in different oxygen species such as O^{2-} and O^{-}. As a result of charge transfer, a depletion layer is formed beneath the oxide surface, thus leading to a positive shift in the V_{TH} of the transistor. Because our devices use a back-channel structure without a passivation layer covering it, the influence of the ambient atmosphere cannot be excluded [58–60].

Table 2. Summary of stretched-exponential fitting parameters for the PBS conditions of In_2O_3 TFTs under different annealing atmospheres.

Annealing atmosphere	ΔV_{TH0} (V)	τ (s)	β
O_2	10.97	1.78×10^4	0.31
Ar	6.12	2.79×10^3	0.26
FG	5.56	4.60×10^3	0.30
N_2	5.67	4.45×10^3	0.29

4. Conclusion

In this study, the effects of annealing atmospheres (O_2, Ar, FG, and N_2) on the structural and electrical properties of room-temperature sputtered In_2O_3 thin films as active channel layers were investigated. All annealed In_2O_3 thin films exhibit polycrystalline properties with high transparency and optical band gap of 3.71 eV. The annealing atmosphere has a significant effect on the electrical properties and bias stability of In_2O_3 TFTs, which is mainly attributed to significant changes in oxygen-related species, particularly V_O and O–H/C–O. The measured μ_{FE} and SS values of the TFTs annealed under different atmospheres were in the order of O_2 (lowest) to Ar, FG, and N_2 (highest). In the same order, the V_{TH} of TFTs became increasingly negative. This was mainly attributed to the higher electron concentration caused by the higher V_O concentration in the In_2O_3 active channel layer. All annealed In_2O_3 TFTs exhibit high mobilities (>40 $cm^2\ V^{-1}s^{-1}$) and microampere level of I_D. The O_2-, Ar-, and FG-annealed In_2O_3 TFTs exhibit clear transfer characteristics ($I_{on}/I_{off} \sim 10^8$) because of a proper modulation of V_O in these In_2O_3 thin films. However, the N_2-annealed TFT exhibits undesired switching properties that are not completely depleted at a reasonable gate bias because of a high carrier concentration caused by excess V_O. In addition, the ΔV_{TH} values observed in the PBS tests for the FG-, and N_2-annealed TFTs were smaller than those for the O_2-, Ar-annealed TFTs, which is attributed to the lower density of O–H/C–O groups in the In_2O_3 active channel layer. Charge trapping at the channel/insulator interface was considered to be the main factor contributing to PBS instability, and the ΔV_{TH} observed during the PBS tests agreed well with the stretched exponential equation. Our study suggests that the annealing of sputtered In_2O_3 thin films is an effective approach to achieve high- performance TFTs with high mobility and controllable V_{TH}. Considering the strong influence of the annealing atmosphere on the electrical properties of In_2O_3 TFTs, careful selection of the annealing atmosphere is necessary.

Data availability statements

All data that support the findings of this study are included within the article (and any supplementary files).

Acknowledgments

This work was supported by KAUST Baseline Fund BAS/1/1664-01-01, Impact Acceleration Fund REI/1/5124-01-01, Near-term Grand Challenge Grant REI/1/4999-01-01, Semiconductor Initiative Grant REP/1/5314-01-01.

ORCID iDs

Na Xiao https://orcid.org/0000-0002-2614-434X
Saravanan Yuvaraja https://orcid.org/0000-0001-9187-0543
Xiao Tang https://orcid.org/0000-0002-0138-7206
Xiaohang Li https://orcid.org/0000-0002-4434-365X

References

[1] Hara Y, Kikuchi T, Kitagawa H, Morinaga J, Ohgami H, Imai H, Daitoh T and Matsuo T 2018 IGZO-TFT technology for large-screen 8K display *J. Soc. Inf. Disp.* **26** 169–77
[2] Striakhilev D, Park B and Tang S-J 2021 Metal oxide semiconductor thin-film transistor backplanes for displays and imaging *MRS Bull.* **46** 1063–70
[3] Wang W S and Zhu L Q 2023 Recent advances in neuromorphic transistors for artificial perception applications *Sci. Technol. Adv. Mater.* **24** 10–41
[4] Ruan D-B, Liu P-T, Chen Y-H, Chiu Y-C, Chien T-C, Yu M-C, Gan K-J and Sze S M 2019 Photoresponsivity enhancement and extension of the detection spectrum for amorphous oxide semiconductor based sensors *Adv. Electron. Mater.* **5** 1800824
[5] Zhang J *et al* 2022 Ultra-wide bandgap semiconductor Ga_2O_3 power diodes *Nat. Commun.* **13** 3900
[6] Kimura M 2019 Emerging applications using metal-oxide semiconductor thin-film devices *Jpn. J. Appl. Phys.* **58** 090503
[7] Jeon Y, Lee D and Yoo H 2022 Recent advances in metal-oxide thin-film transistors: flexible/stretchable devices, integrated circuits, biosensors, and neuromorphic applications *Coatings* **12** 204
[8] Zheng Z, Liang W, Lin R, Hu Z, Wang Y, Lu H, Zhong W, Shen S and Pan Y 2023 Facile synthesis of zinc indium oxide nanofibers distributed with low content of silver for superior antibacterial activity *Small Struct.* **4** 2200291
[9] Kamiya T, Nomura K and Hosono H 2010 Present status of amorphous In–Ga–Zn–O thin-film transistors *Sci. Technol. Adv. Mater.* **11** 044305
[10] Nomura K, Ohta H, Takagi A, Kamiya T, Hirano M and Hosono H 2004 Room-temperature fabrication of transparent flexible thin-film transistors using amorphous oxide semiconductors *Nature* **432** 488–92
[11] Um J G, Jeong D Y, Jung Y, Moon J K, Jung Y H, Kim S, Kim S H, Lee J S and Jang J 2019 Active-matrix GaN μ-LED display using oxide thin-film transistor backplane and flip chip LED bonding *Adv. Electron. Mater.* **5** 1800617
[12] Wei Shih C, Chin A, Fu Lu C and Fang Su W 2016 Remarkably high mobility ultra-thin-film metal-oxide transistor with strongly overlapped orbitals *Sci. Rep.* **6** 19023
[13] Choi J Y and Lee S Y 2017 Comprehensive review on the development of high mobility in oxide thin film transistors *J. Korean Phys. Soc.* **71** 516–27

[14] Magari Y, Kataoka T, Yeh W and Furuta M 2022 High-mobility hydrogenated polycrystalline $In_2O_3(In_2O_3{:}H)$ thin-film transistors *Nat. Commun.* **13** 1078
[15] Kang M H, Armitage J, Andaji-Garmaroudi Z and Sirringhaus H 2021 Surface passivation treatment to improve performance and stability of solution-processed metal oxide transistors for hybrid complementary circuits on polymer substrates *Adv. Sci.* **8** 2101502
[16] Cho S, Yang J-H, Oh J G, Cho S-H, Hwang C-S, Jang J and Nam S 2017 The role of oxygen in dramatically enhancing the electrical properties of solution-processed Zn–Sn–O thin-film transistors *J. Mater. Chem.* C **5** 6521–6
[17] Fortunato E, Barquinha P and Martins R 2012 Oxide semiconductor thin-film transistors: a review of recent advances *Adv. Mater.* **24** 2945–86
[18] Cha H-S, Jeong H-S, Hwang S-H, Lee D-H and Kwon H-I 2020 Electrical performance and stability improvements of high-mobility indium–gallium–tin oxide thin-film transistors using an oxidized aluminum capping layer of optimal thickness *Electronics* **9** 2196
[19] Wang X, Zhang J, Wang Z, Lin Z, Shen S and Zhong W 2023 Fabricating Ru single atoms and clusters on CoP for boosted hydrogen evolution reaction *Chin. J. Struct. Chem.* **42** 100035
[20] Robertson J and Guo Y 2014 Light induced instability mechanism in amorphous InGaZn oxide semiconductors *Appl. Phys. Lett.* **104** 162102
[21] Reed A, Stone C, Roh K, Song H W, Wang X, Liu M, Ko D-K, No K and Lee S 2020 The role of third cation doping on phase stability, carrier transport and carrier suppression in amorphous oxide semiconductors *J. Mater. Chem.* C **8** 13798–810
[22] Han S, Im C, Kim Y S and Kim C 2022 Indium and tin doping of zinc oxide film by cation exchange and its application to low-temperature thin-film transistors *Adv. Mater. Interfaces* **9** 2200190
[23] Yang D G, Kim H D, Kim J H, Lee S W, Park J, Kim Y J and Kim H-S 2017 The effect of sputter growth conditions on the charge transport and stability of In-Ga-Zn-O semiconductors *Thin Solid Films* **638** 361–6
[24] Zhang L 2021 The effect of post-metal annealing on the electrical performance and stability of two-step-annealed solution-processed In_2O_3 thin film transistors *Curr. Appl. Phys.* **23** 19–25
[25] Charnas A, Si M, Lin Z and Ye P D 2021 Enhancement-mode atomic-layer thin In_2O_3 transistors with maximum current exceeding 2 A/mm at drain voltage of 0.7 V enabled by oxygen plasma treatment *Appl. Phys. Lett.* **118** 052107
[26] Liu W-S, Hsu C-H, Jiang Y, Lai Y-C and Kuo H-C 2022 Improving device characteristics of dual-gate IGZO thin-film transistors with Ar–O_2 mixed plasma treatment and rapid thermal annealing *Membranes* **12** 49
[27] Aikawa S, Nabatame T and Tsukagoshi K 2013 Effects of dopants in InO_x-based amorphous oxide semiconductors for thin-film transistor applications *Appl. Phys. Lett.* **103** 172105
[28] Hu S *et al* 2021 Study of the correlation between the amorphous indium-gallium-zinc oxide film quality and the thin-film transistor performance *Nanomaterials* **11** 522
[29] Jeong H-S, Cha H S, Hwang S H and Kwon H-I 2020 Effects of annealing atmosphere on electrical performance and stability of high-mobility indium-gallium-tin oxide thin-film transistors *Electronics* **9** 1875
[30] Tang T *et al* 2023 Analysis of the annealing budget of metal oxide thin-film transistors prepared by an aqueous blade-coating process *Adv. Funct. Mater.* **33** 2207966
[31] Peng C, Yang S, Pan C, Li X and Zhang J 2020 Effect of two-step annealing on high stability of a-IGZO thin-film transistor *IEEE Trans. Electron Devices* **67** 4262–8
[32] Noviyana I, Lestari A D, Putri M, Won M-S, Bae J-S, Heo Y-W and Lee H Y 2017 High mobility thin film transistors based on amorphous indium zinc tin oxide *Materials* **10** 702
[33] Rim Y S, Choi H-W, Kim K H and Kim H J 2016 Effects of structural modification via high-pressure annealing on solution-processed InGaO films and thin-film transistors *J. Phys. D: Appl. Phys.* **49** 075112
[34] Fu R, Yang J, Zhang Q, Chang W-C, Chang C-M, Liu P-T and Shieh H-P D 2018 Annealing effect on amorphous indium-zinc-tungsten-oxide thin-film transistors *2018 IEEE 2nd Electron Devices Technology and Manufacturing Conf. (EDTM)* pp 334–6
[35] Arulkumar S, Parthiban S and Kwon J Y 2022 The influence of post-annealing temperature on indium-silicon oxide thin film transistors *Mater. Sci. Semicond. Process.* **145** 106665
[36] Yuan Z, Zhu X, Wang X, Cai X, Zhang B, Qiu D and Wu H 2011 Annealing effects of In_2O_3 thin films on electrical properties and application in thin film transistors *Thin Solid Films* **519** 3254–8
[37] Si M, Charnas A, Lin Z and Ye P D 2021 Enhancement-mode atomic-layer-deposited In_2O_3 transistors with maximum drain current of 2.2A/mm at drain voltage of 0.7V by low-temperature annealing and stability in hydrogen environment *IEEE Trans. Electron Devices* **68** 1075–80
[38] Keller J, Aijaz A, Gustavsson F, Kubart T, Stolt L, Edoff M and Törndahl T 2016 Direct comparison of atomic layer deposition and sputtering of $In_2O_3{:}H$ used as transparent conductive oxide layer in $CuIn_{1-x}Ga_xSe_2$ thin film solar cells *Sol. Energy Mater. Sol. Cells* **157** 757–64
[39] Juneja N, Tutsch L, Feldmann F, Fischer A, Bivour M, Moldovan A and Hermle M 2019 Effect of hydrogen addition on bulk properties of sputtered indium tin oxide thin films *AIP Conf. Proc.* **2147** 040008
[40] Tauc J, Grigorovici R and Vancu A 1966 Optical properties and electronic structure of amorphous germanium *Phys. Status Solidi* b **15** 627–37
[41] Kim H, Gilmore C M, Piqué A, Horwitz J S, Mattoussi H, Murata H, Kafafi Z H and Chrisey D B 1999 Electrical, optical, and structural properties of indium-tin-oxide thin films for organic light-emitting devices *J. Appl. Phys.* **86** 6451–61
[42] Ma Q, Zheng H-M, Shao Y, Zhu B, Liu W-J, Ding S-J and Zhang D W 2018 Atomic-layer-deposition of indium oxide nano-films for thin-film transistors *Nanoscale Res. Lett.* **13** 4
[43] Ji X, Yuan Y, Yin X, Yan S, Xin Q and Song A 2022 High-performance thin-film transistors with sputtered IGZO/Ga_2O_3 heterojunction *IEEE Trans. Electron Devices* **69** 6783–8
[44] Nguyen T T T, Renault O, Aventurier B, Rodriguez G, Barnes J P and Templier F 2013 Analysis of IGZO thin-film transistors by XPS and relation with electrical characteristics *J. Disp. Technol.* **9** 770–4
[45] Park S, Bang S, Lee S, Park J, Ko Y and Jeon H 2011 The effect of annealing ambient on the characteristics of an indium-gallium-zinc oxide thin film transistor *J. Nanosci. Nanotechnol.* **11** 6029–33
[46] Li S, Tian M, Gao Q, Wang M, Li T, Hu Q, Li X and Wu Y 2019 Nanometre-thin indium tin oxide for advanced high-performance electronics *Nat. Mater.* **18** 1091–7
[47] Kamiya T, Nomura K and Hosono H 2009 Origins of high mobility and low operation voltage of amorphous oxide TFTs: electronic structure, electron transport, defects and doping *J. Disp. Technol.* **5** 273–88
[48] Hu M, Xu L, Zhang X, Hao H, Zong S, Chen H, Song Z, Luo S and Zhu Z 2023 High mobility amorphous InSnO thin film transistors via low-temperature annealing *Appl. Phys. Lett.* **122** 033503

[49] Kamiya T, Nomura K and Hosono H 2009 Electronic structures above mobility edges in crystalline and amorphous In-Ga-Zn-O: percolation conduction examined by analytical model *J. Disp. Technol.* **5** 462–7
[50] Takagi A, Nomura K, Ohta H, Yanagi H, Kamiya T, Hirano M and Hosono H 2005 Carrier transport and electronic structure in amorphous oxide semiconductor, a-$InGaZnO_4$ *Thin Solid Films* **486** 38–41
[51] Wang R X, Beling C D, Fung S, Djurišić A B, Ling C C and Li S 2005 Influence of gaseous annealing environment on the properties of indium-tin-oxide thin films *J. Appl. Phys.* **97** 033504
[52] Charnas A, Si M, Lin Z and Ye P D 2022 Improved stability with atomic-layer-deposited encapsulation on atomic-layer In_2O_3 transistors by reliability characterization *IEEE Trans. Electron Devices* **69** 5549–55
[53] Abdullah I, Macdonald J E, Lin Y-H, Anthopoulos T D, Salahr N H, Kakil S A and Muhammadsharif F F 2020 Bias stability of solution-processed In_2O_3 thin film transistors *J. Phys. Mater.* **4** 015003
[54] Cross R B M and De Souza M M 2006 Investigating the stability of zinc oxide thin film transistors *Appl. Phys. Lett.* **89** 263513
[55] Young N D and Gill A 1990 Electron trapping instabilities in polycrystalline silicon thin film transistors *Semicond. Sci. Technol.* **5** 72
[56] Dao V A, Trinh T T, Jang K, Ryu K and Yi J 2013 Trapping time characteristics of carriers in a-InGaZnO thin-film transistors fabricated at low temperatures for next-generation displays *J. Electron. Mater.* **42** 711–5
[57] Yoon S-J, Seong N-J, Choi K, Shin W-C and Yoon S-M 2018 Investigations on the bias temperature stabilities of oxide thin film transistors using In–Ga–Zn–O channels prepared by atomic layer deposition *RSC Adv.* **8** 25014–20
[58] Jeong J K, Won Yang H, Jeong J H, Mo Y-G and Kim H D 2008 Origin of threshold voltage instability in indium-gallium-zinc oxide thin film transistors *Appl. Phys. Lett.* **93** 123508
[59] Park J-S, Jeong J K, Chung H-J, Mo Y-G and Kim H D 2008 Electronic transport properties of amorphous indium-gallium-zinc oxide semiconductor upon exposure to water *Appl. Phys. Lett.* **92** 072104
[60] Kang D, Lim H, Kim C, Song I, Park Y, Park J and Chung J 2007 Amorphous gallium indium zinc oxide thin film transistors: sensitive to oxygen molecules *Appl. Phys. Lett.* **90** 192101